Journal of Zhejiang University-SCIENCE A (Applied Physics & Engineering) 2022 23(1):40-54
www.jzus.zju.edu.cn; www.springer.com/journal/11582
E-mail: jzus_a@zju.edu.cn

Research Article

https://doi.org/10.1631/jzus.A2100188

A new technique for high-fidelity cutting technology for hydrate samples

Hai ZHU[1], Jia-wang CHEN[1,3]✉, Zi-qiang REN[1], Pei-hao ZHANG[1], Qiao-ling GAO[1], Xiao-ling LE[1], Chun-ying XU[2], Kai HE[1], Peng ZHOU[1], Feng GAO[1], Yu-ping FANG[1]

[1]*Institute of Ocean Engineering and Technology, Ocean College, Zhejiang University, Zhoushan 316021, China*
[2]*Key Lab of Digital Signal and Image Processing of Guangdong Province, School of Engineering, Shantou University, Shantou 515063, China*
[3]*Southern Marine Science and Engineering Guangdong Laboratory (Guangzhou), Guangzhou 511458, China*

Abstract: Designing a high-fidelity cutting device is one of the difficulties in hydrate samples pressure-holding transfer. Due to the limitations of the existing mechanical system, there is much damage to the cut surface of hydrate samples, with many chips produced, which seriously affects the quality of samples. In this paper, a new cutting device utilizes two servo motors to achieve a high degree of automation. Using the Archimedes spiral, it achieves low disturbance of the cut surface and provides accurate control of the process. In addition, due to the operation of the sample long-stroke push unit, cutting hydrate samples of any length with almost no chips within a short cutting time can be achieved. Laboratory and sea tests have achieved all design requirements of the equipment and strongly demonstrate its benefit and stability. It is concluded that this new high-fidelity cutting technology is practically efficient. The physical state of the hydrate can be maintained to the greatest extent, and thus the new equipment provides significant support for the exploration and development of hydrate resources.

Key words: High-fidelity; Cutting technology; Hydrate samples; Automation

1 Introduction

Subsea sampling can accelerate the efficiency and accuracy of the exploration and geological surveys of marine resources. It can save costs, and provide good social and economic benefits (Zhao et al., 2017; Yoneda et al., 2019). Taking natural gas hydrates as an example, sampling a natural gas hydrate to obtain relevant parameters can provide theoretical support for its commercial exploitation (Li et al., 2018; Ye et al., 2018, 2020). Drilling for samples is a conventional technique in marine resource exploration and geological investigation (Tsuchiya et al., 2019; Hoang et al., 2021). After the hydrate has been sampled, the sampler is transported to a ship. The sample tube is removed from the sampler and is sent to the pressure maintaining transfer device for pressure transfer, test analysis, cutting, and storage. High-fidelity samplers are an established instrument for marine researchers because of their ability to maintain the characteristics and composition of samples (Parkes et al., 2009; Moore et al., 2020; Wang et al., 2020). The hydrate in the samplers would decompose with the decrease of external pressure and increase of temperature before it reaches sea level (Hyodo et al., 2014), if there were no pressure maintenance mechanism, the resulting gas expanding inside the hydrate would destroy its original structure (Dai and Santamarina, 2014). Therefore, maintaining the original pressure and temperature at the sampling point is very important for hydrate research (Zhang et al., 2019). It should be noted that getting high-fidelity hydrate samples to the workboat deck is not all that needs to be done before laboratory analysis (Gao et al., 2020). The samplers are not suitable for long-term core storage, and a sample storage tank is the best core storage choice. Therefore, the process from the samplers to the storage chamber (including cutting) must ensure that any fluctuation in the storage environment parameters of the hydrate samples does not cause structural and state changes in them.

✉ Jia-wang CHEN, arwang@zju.edu.cn
Hai ZHU, https://orcid.org/0000-0002-4681-163X
Jia-wang CHEN, https://orcid.org/0000-0002-6351-0062

Received Apr. 20, 2021; Revision accepted July 12, 2021;
Crosschecked Dec. 2, 2021

On the one hand, the samplers usually need to follow the design principle of making the obtained sample have the highest research value (in general, the longer the sampling tube, the higher the research value); but on the other hand, the size of the sample tube is not compatible with most laboratory analytical instruments, such as computed tomography (CT) scanners. The solution is to cut the hydrate sampling tube into segments of the required size, transfer them to the sample storage tank, and finally place the sample storage tank in the laboratory analytical instrument. Core sample processing needs to be completed before laboratory analysis, and for that high-fidelity cutting technology of the hydrate sample is an essential component in many processing steps and an essential guarantee of sample quality (Gao et al., 2020).

At present, there is a mature and commercially available comprehensive pressure protection test system (pressure core analysis and transfer system (PCATS)) (Priest et al., 2015), which has a wide range of functions, including long-stroke push, pressure-holding cutting, temperature control system, secondary sampling, and non-destructive measurement. In the cutting unit alone, PCATS first uses a rotating cutter to cut the plastic casing and then uses a reciprocating saw cutter to cut the sediment core. However, the system has many disadvantages, such as manual control, frequent loading and unloading for multiple cuts, and difficulty of precision control. The cutting environment of the hydrate sample tubes is a confined space at high pressure and low temperature (Zhu et al., 2018), which brings significant difficulties for power transmission, cutting process control, and core debris cleaning.

Given the shortcomings of PCATS, our team has developed a new set of core pressure-maintaining transfer devices. The hydrate core sample tube is 2 m long and 48.5 mm in diameter. The sample tube is made of polyvinyl chloride (PVC) and contains a whole section of hydrate. The length of the whole pressure retaining transfer system is 18 m, and the outer diameter varies according to the function of each part, but the inner diameter is basically 50 mm. Its structure is shown in Fig. 1.

Combining a pressure and temperature maintaining unit and a long-stroke push unit, a pressure-holding transfer system for the hydrate samples is formed. The pressure and temperature maintaining unit is responsible for the temperature and pressure regulation of the entire pressure-holding transfer system for the hydrate samples, and controls the heat exchange using compressors, reservoirs, evaporators, condensers, and expansion valves, with an accuracy of 0.5 °C (Zhang et al., 2019). A stable external environment (the same temperature and pressure as the sampling point) is provided for the high-fidelity cutting device. The long-stroke push unit is responsible for the movement and precise positioning of the sample tube within the pressure-holding transfer system. In conjunction with the high-fidelity cutting unit, the sample tube can be cut to almost any length (Ren et al., 2020). With these two units, both the long-term stability of temperature and pressure and the smooth long-stroke transfer of sampling tubes can be achieved.

2 Mechanical structure design

2.1 Overall design of the high-fidelity cutting device

Under 30 MPa pressure and 2–4 °C temperature conditions, the cutting device should cut the hydrate

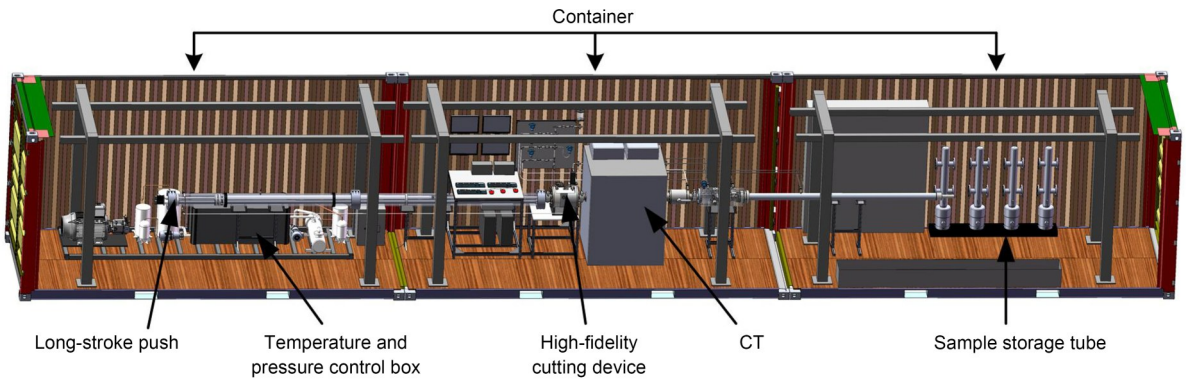

Fig. 1 Overall pressure maintaining transfer device

sample tubes smoothly and quickly without interference. Common pipe cutting methods are not carried out in pressurized enclosed spaces, so the restriction on radial dimensions is relatively weak, and the cutting environment is not filled with water. Cutting methods available include grinding wheel cutting, electrical spark cutting, and high-pressure water cutting (Toussaint, 2008; Hayashi et al., 2014). However, these methods are not applicable due to the particulars of the working environment and the unstable nature of the hydrates. The problems to be solved in high-fidelity cutting technology include temperature and pressure fluctuation, the disturbance of cutting to the sample, dynamic sealing of moving parts, control of the cutting process, and compatibility of cutting objects. An illustration of the high-fidelity cutting device is shown in Fig. 2, and the design parameters for the equipment are:

(1) Working pressure: 30 MPa;

(2) Operating temperature: 2–4 °C;

(3) Pressure and temperature fluctuation during transfer: ⩽10%;

(4) Single cutting time: ⩽3 min;

(5) No sample contamination from cutting operations;

(6) Controllable cutting process and calculable cutter position.

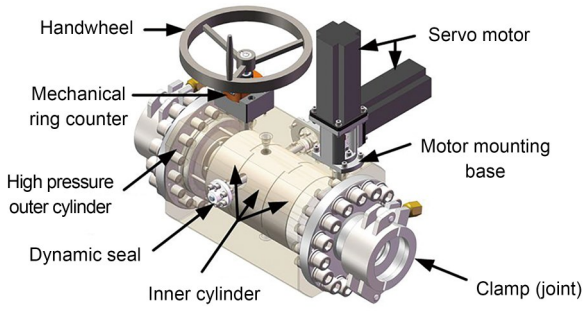

Fig. 2 High-fidelity cutting device

To achieve less sample disturbance than in PCATS, full-range rotary cutting is used instead of reciprocating cutting and servo motors are used instead of handwheels to achieve better cutting process control. In addition, an independent anti-blocking structure is designed to solve the problems of frequent loading and unloading. The high-fidelity cutting device in the sampling tube includes a clamping mechanism and a cutting mechanism. The connection between the high-fidelity cutting device and other parts of the hydrate samples pressure-holding transfer system is designed in a quick-connect form to facilitate offshore operations and therefore clamps and end-cap flanges are included at both ends of the device. Also, two servo motors are used to drive the cutting mechanism, and a handwheel is used to drive the clamping mechanism. To achieve a high-pressure dynamic seal, and in consideration of the ease of assembly of the remaining parts, some auxiliary parts are designed. The parameters of the high-fidelity cutting device are shown in Table 1.

2.2 Internal structure composition

The high-fidelity cutting device performs two functions, clamping and cutting, which are realized by two mechanisms with the same principle but slightly different structures. Two servo motors control the cutting and a handwheel controls the clamping. An electronic control system matched with the cutting operation is designed separately and is mainly used to control the rotation direction and speed of the servo motors. Details will be given later in this paper. Besides, the adoption of an Archimedes spiral makes it possible to control the circumferential rotation speed and radial feed speed of the cutter accurately. The electronic control system realizes start-stop, emergency braking, and automatic reset of the cutting. It is also used to calculate the knife position in real-time. The

Table 1 Parameters of the high-fidelity cutting device

Parameter	Description
Total length of high-fidelity cutting device, L (mm)	618
Total width of high-fidelity cutting device, M (mm)	548
Total height of high-fidelity cutting device, H (mm)	518
Main materials of other parts	17-4PH
Alternating current (AC) servo motor model	DEL ECMA-J10807SS
High performance motion control type AC servo drive	DELTA ASD-A2-0743-M
Power of high-fidelity cutting device, P (W)	1500
Input voltage, U (V)	380

low chip and anti-blocking design make possible multiple cuts without removing the knife. The cutting device section is shown in Fig. 3.

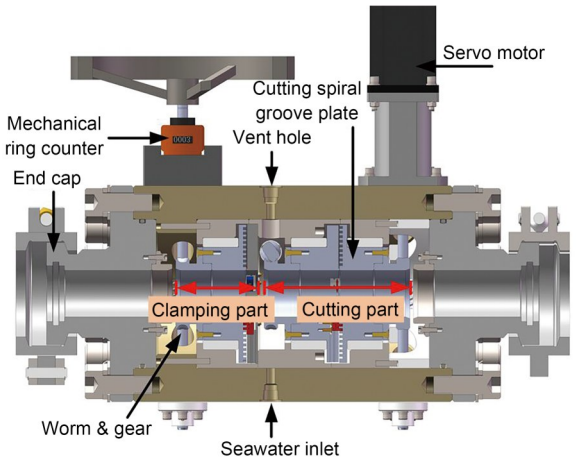

Fig. 3 Cutting device section

The sample tube is very fragile as the wall thickness is only 1.5 mm (Yi et al., 2017; Gao et al., 2020). To prevent the sample tube from breaking, the clamping mechanism must not exert too much force. Although a servomotor and sensor design would be more automated, it would complicate the structure, and additional control programs would be required, increasing the uncertainty. Because the required clamping accuracy is not high, the movement of the clamping mechanism can be quickly and conveniently controlled by installing a handwheel on the transmission worm.

Fig. 4 is the high-fidelity cutting device's primary working mechanism for clamping and cutting.

As can be seen from the clamping mechanism components, the clamping part consists of a clamping jaw limit plate fixed with countersunk bolts and a slotted plate with helical lines. The clamping jaws are fixed between the two. Rotating the handwheel drives the worm wheel to rotate, thereby driving the clamping spiral groove disk to rotate, and the clamping jaws are fed or retracted accordingly. The mechanical counter installed on the clamping device provides a reference for the degree of clamping. The clamping jaw head is designed as a toothed shape for better fixing the thin-walled sampling tube. The experiment also shows that the clamping effect can achieve the preset effect without slippage. The most significant difference between the cutting mechanism and the clamping mechanism is that the former has an additional drive input. The worm gear and worm parameters of cutting mechanism are shown in Table 2.

2.3 Quality section guarantee method

The two pairs of worm gears connect the cutting limit plate and the cutting spiral groove plate respectively. They rotate in the same direction but at different speeds. The speed of the cutter limit disc (V1) determines the circumferential rotation speed, and the speed difference between the plates determines the feed and return speed of cutting. For example, if the cutter head speed V1 (anti-clockwise) is greater than V2 (clockwise), the tool will feed; if the cutter head speed V1 (anti-clockwise) is less than V2 (clockwise), the cutter will retract. The rotation direction of V1 and V2 above is the same as shown in Fig. 5.

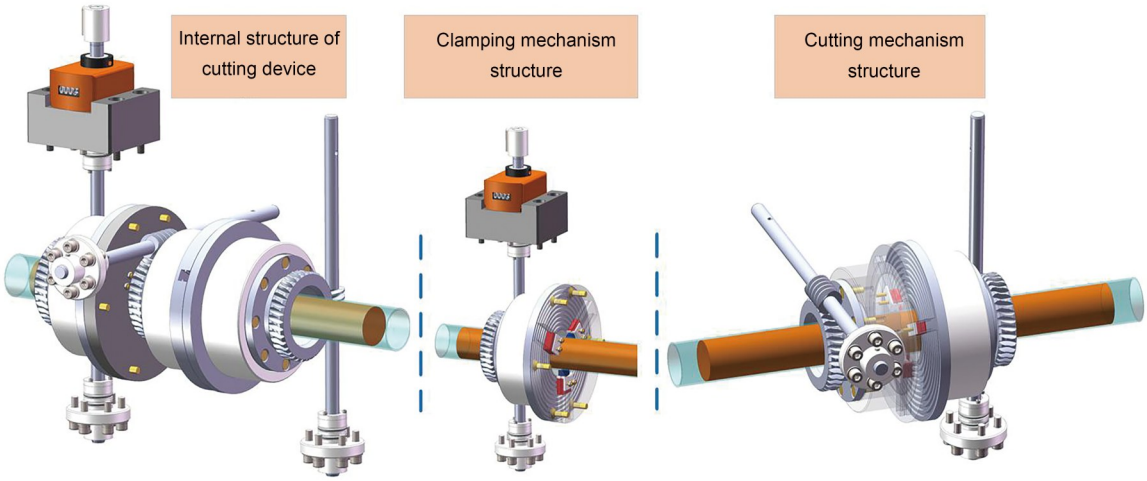

Fig. 4 Schematic realization of the high-fidelity cutting device

Table 2 Worm gear and worm parameters of cutting mechanism

Parameter	Description	
	Worm gear	Worm
Axial modules, m_n	2	2
Number of worm teeth or heads, z	36	2
Tooth angle (°)	20	20
Coefficient of addendum height	1	1
Axial modulus, γ (°)	12.53	12.53
Rotation direction	Right	Right
Radial displacement coefficient, x_n	0	0
Transmission ratio, i	18	18
Transmission center distance (mm)	45	45

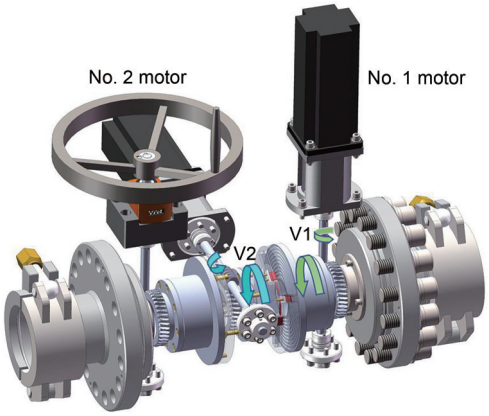

Fig. 5 Direction of rotation

As shown in Fig. 6, the key to ensure the quality of the cutting surface lies in application of an Archimedes spiral in this cutting equipment. The Archimedes spiral is an iso-velocity ratio spiral because it advances an equal distance with each rotation cycle. This feature ensures a constant feed speed and high quality of the core sample cut surface due to the circumferential rotation of the cutter (Kamruzzaman and Dhar, 2009; Saelzer et al., 2020; Zhu et al., 2020). The Archimedean spiral is determined by the following parametric equation:

$$\begin{cases} x = \dfrac{p\cos(\theta)}{\pi} + \dfrac{p\theta\sin(\theta)}{\pi}, \\ y = \dfrac{p\sin(\theta)}{\pi} - \dfrac{p\theta\cos(\theta)}{\pi}, \end{cases} \tag{1}$$

where p represents the corresponding increase in the polar diameter of the Archimedes spiral for each revolution, and its value in this equipment is 2.5 mm. θ represents the polar angle of Archimedes spiral.

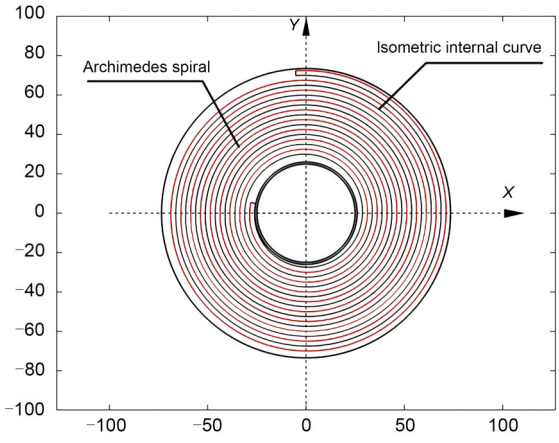

Fig. 6 Surface curve of spiral grooved plate (unit: mm)

The isometric internal curve is 1.25 mm apart from the Archimedes spiral. According to the different usages of clamping the spiral groove plate and cutting the spiral groove plate, the parameter equation interval of the Archimedes spiral is set as [12.39π, 26.55π] and [11.43π, 29.02π].

2.4 Realization of high-pressure dynamic seal and anti-silting design of the cutter

The structure of the high-pressure rotating seal is shown in Fig. 7. The sealing structure includes Glyd-ring, O-ring, plastic bearing, bearing copper sleeve, Glyd-copper sleeve, thrust piece, and seal gland. The thrust piece eliminates the lateral force of the worm. Because of the imbalance of internal and external pressures, the high internal pressure will eject the Glyd-copper sleeve of the bearing outwards, so a seal gland is used for corresponding low dissipation. The dynamic seal of the worm is achieved using plastic

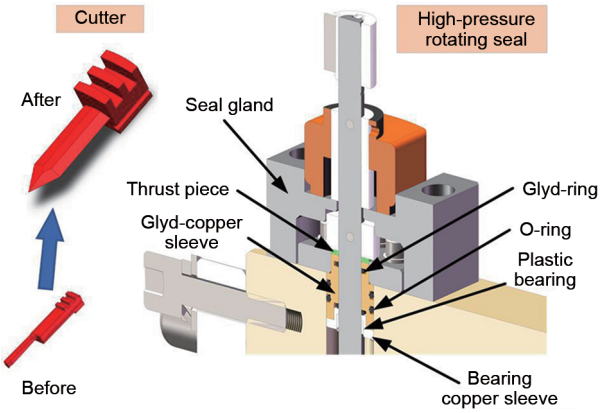

Fig. 7 High-pressure dynamic seal and cutter improvement device

bearings and Glyd-rings, while the O-rings guarantee the static seal. The dimensions of the above seals are determined in accordance with the design manual, and the design calculations are carried out.

Tools are an essential basis for cutting, so their structural design is extremely important. We have made several trial cuts and accordingly have made several improvements that have resulted in almost disturbance-free and chip-free cutting. The cutting tool is designed with reference to the lathe tool, but due to the low strength of the thin-walled plastic pipe, the sample tube will shake around the center axis of the cylinder in the case of a long cantilever (Zhu et al., 2020). Therefore, the end of the cutter needs to be designed in a spire style, which facilitates the cutter fitting into the sample tube (Yi et al., 2017; Lukin et al., 2020). The cutting surface needs to be as smooth as possible, so the thickness of the cutting knife needs to be minimized. In order to reduce shaking during cutting, the edge of the cutting knife should be sharp. The expected cutting effect can be achieved by installing such a cutter on the lathe turret but, during assembly, the cutter cannot rotate flexibly in the grooved plate, so we increased the tolerance and achieved a smooth rotation of the cutter in the grooved plate.

Considering that the current cutting device adopts the combination of spiral groove plates and limit plates, there is a large gap between them, and chips will inevitably occur during cutting (Zhu et al., 2018). The presence of small stones and sludge in the sample makes it possible for impurities to enter the gap, leading to the tool's rotary blockage. A set of anti-silting structures is designed separately based on spiral groove plates to prevent silt and small stones from entering the spiral groove plates and affecting cutting (Pang et al., 2019). The anti-blockage design mainly involves two kinds of cutters: cutter and clamping jaw. A similar anti-blockage principle is adopted to modify the equipment according to the shape of the cutters. A closed ring face is formed by using the boss of the limit plates and the spiral groove plates. Also, due to the movement of the cutters, a gap in the stroke is formed, and the anti-siltation of this gap is achieved by using a plug. For plug installation, slots, threaded mounting holes, and cutter holes are designed on the plug. Since the sampling tube needs to be moved in the pressure-retaining cutting device, the plug is designed as a curved surface. Besides, to avoid the tool rushing through the plug and pushing the plug out, stroke determination is required for the spiral grooved plates. The anti-blocking design is shown in Fig. 8.

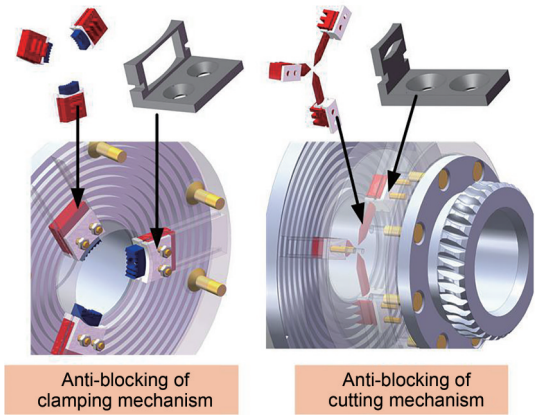

Fig. 8 Anti-blocking design

3 Electronic control design

The pressure-holding transfer system's control system for the hydrate samples includes the upper machine monitoring software, deck high-voltage power supply, central control system board, power conversion module, motor control system, temperature/pressure sensor, and other parts. The overall composition of the control system is shown in Fig. 9.

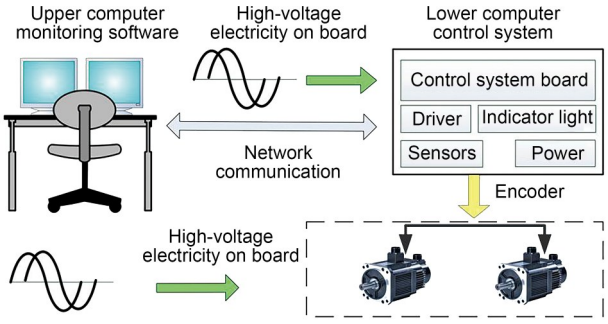

Fig. 9 Overall composition of the control system

The shipboard 440-V alternating current (AC) is converted to 380-V AC and 220-V AC through the distribution cabinet and then to direct current (DC) with different voltages. The above power supply is used to supply the motor, temperature and pressure maintenance unit, control system boards, relay, and chips. Communication data between the control board and the upper computer is transmitted via the network

interface and twisted-pair wire, and the control board controls the motor driver through the CANopen protocol to control the operation of the motors. The control panel gathers the collected data, such as motor speed and torque, and sends them to the upper computer by a communication protocol. They are displayed on the monitoring screen as a dial or curve drawn by the upper computer. The control commands of the motor and the commands to switch on and off the valves sent by the upper computer will also be sent to the control board through the communication protocol. The control board controls all parts to perform corresponding actions to complete the upper computer's instructions.

As shown in Fig. 10, the hardware composition of the industrial computer mainly includes an AC-DC power supply system, control board system circuit, and motor driver. As shown in Fig. 10, the AC-DC power supply system converts 380-V AC input to 220-V AC, then 220-V AC to 24-V DC for power supply of the control system board, valves, and lights. Also, 24-V DC is converted to 12-V DC and 3.3-V DC for current supply to relays, operational amplifier chips, central processing unit (CPU) chips, and fans. In the control board system, besides the CPU's primary circuit, a network hardware circuit is also included to achieve network communication with the host computer. The current/voltage (I/V) conversion circuit converts the 4–20 mA current signal sent by the sensor into a 1–5 V voltage signal. The analog to digital (AD) acquisition circuit reads the converted voltage signal and fits it into the intuitive temperature and pressure display. In addition, the CPU controls the switching on and off of relay groups through input/output (I/O), which further controls various external devices. The motor driver occupies most of the space of the whole industrial control cabinet. By setting the motor driver as a controller area network (CAN) interface of each node and control system, CANopen local area network (LAN) is formed to control the motor. Two drivers are used to control the two motors throughout the transfer system for cutting the core pipe.

As the window to the whole system, the upper computer software is important for human-machine interaction. The development language of the upper computer control software designed in this system is C#, the development environment is in. NET Framework 4.5, and the development software is Visual Studio 2019. The system's software program is based on Windows Forms, and the main application model is in in. NET Framework, with a wide range of graphical desktop applications that are easy to update and deploy. The software program consists of two parts: the first part is the control provided by the platform, dragging it to the specified position of the window, changing the color, size, format, and other data in its attributes as needed, and the system background will automatically generate the corresponding underlying program code; the second part is based on the data protocol uploaded by the control board and the control commands issued by the host computer. The logical classification is completed by analyzing, cutting, and dividing the data, and is dynamically combined with the controls of the first part to form a complete run for the program. The interface layout is completed as shown in Fig. 11.

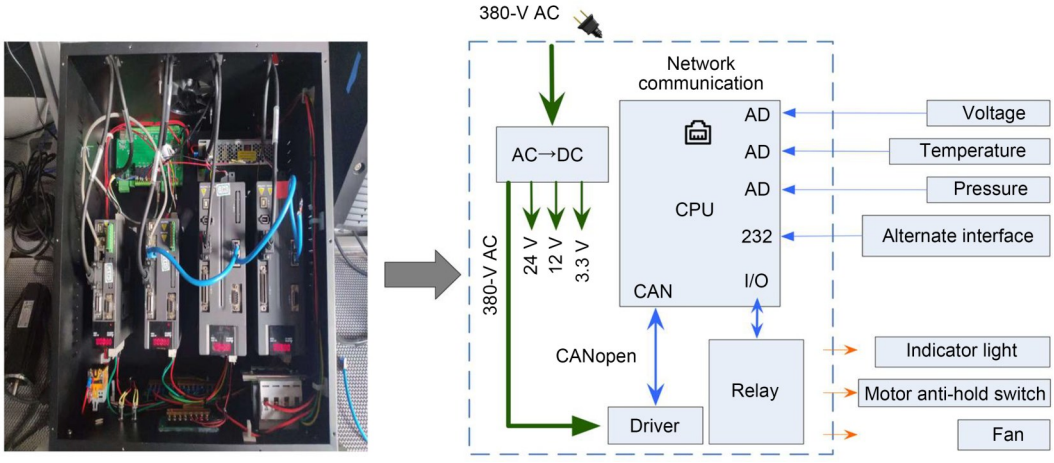

Fig. 10 Hardware composition of industrial computer

Fig. 11 Upper computer interface

The cutting-related parts on the upper computer interface include the following:

1. Dynamic display region for sample handling: this dynamically displays the core sample tube position and provides position information for sample tube cutting.

2. Cutting motors' status display region: this region dynamically displays the speed and torque of the cutting motor on a dial.

3. Cutting control buttons: these regulate the core cutting process in the core tube by multiple control buttons for automatic control.

4. Indicator light region: this displays the running status of the cutting motor, open or closed.

5. Log region: this displays the log preparation of network connection, with a text warning in case of a program operation error.

The internal logic of the whole interface layout includes the reading and clipping of the uploaded data and the dynamic association of the distributed data. The logical process of uploading data involves sending data using a network protocol, judging the frame head and frame tail after receiving, obtaining the data information, saving the data information in the log, and then cutting the data information to display it in each display area. The logic flow of uploading data involves a motor control command input through the cutting control area and other positions and is then sent to the control board of the lower computer through the network interface after splicing. A check code is added, and the data sent can also be saved in the log.

4 Calculations

4.1 Pressure maintaining calculations

Because the internal pressure of the high-fidelity cutting device is up to 30 MPa, the size of the outer barrel involves a choice of the bore diameter, overall length, wall thickness, and material. The sample tube's outer diameter determines the depth of feed required by the tool and the maximum depth of feed for the tool. The outer diameter of the sample tube can roughly determine the bore diameter of the outer cylinder. The corresponding wall thickness is calculated based on the bore diameter, taking into account a safety factor.

It is noted that the wall thickness of the high-pressure outer cylinder should be designed to resist the working environment pressure of 30 MPa, and the wall thickness is calculated by

$$\delta=\frac{P_{\mathrm{c}}D_{\mathrm{i}}}{2[\sigma]^{t}\phi-P_{\mathrm{c}}}, \tag{2}$$

where P_{c} is the ambient pressure during equipment operation, D_{i} is the inner diameter of the high-pressure outer cylinder, $[\sigma]^{t}$ is the allowable stress of materials at design temperature t, and ϕ is the welding coefficient.

Intensity examination was carried out by the following formula:

$$\frac{P_{\mathrm{T}}\left(D_{\mathrm{i}}+\delta_{\mathrm{e}}\right)}{2\delta_{\mathrm{e}}}\leqslant 0.9\phi R_{\mathrm{eL}}, \tag{3}$$

where P_T is the test pressure, δ_e is the effective thickness of the high-pressure outer cylinder, and R_{eL} is the yield strength of its material.

Similar calculations were carried out during the design of the device. The pressure-bearing body of the high-fidelity cutting device is the high-pressure outer cylinder. Aluminum alloy 7075 was chosen, taking into account corrosion resistance, strength, and price. Its parameters are shown in Table 3.

Table 3 Parameters of the high-pressure outer cylinder

Parameter	Description
Length, l (mm)	550
Inner diameter, d (mm)	160
Side length (mm)	232
Material	7075T6
Density, ρ (kg/m^3)	2.81×10^3
Tensile strength, σ_t (Pa)	5.72×10^8
Young's modulus, E (Pa)	7.17×10^{10}
Poisson's ratio, v	0.33

4.2 Force analysis of the cutters

Force analysis of the cutting knife is carried out according to the curve characteristics of the Archimedes spiral, and the power required for cutting can be calculated, providing a reference for motor selection. Fig. 12 shows the force analysis of a cutting knife (Li and Kishawy, 2006). $\boldsymbol{F}_p$ is the friction force on the cutting spiral grooved plate due to the rotation of the cutters; $\boldsymbol{F}_{pr}$ and $\boldsymbol{F}_{pt}$ are the radial and tangential components of $\boldsymbol{F}_p$, respectively; $\boldsymbol{P}$ is the positive pressure of cutter on cutting spiral groove plate; $\boldsymbol{P}_r$ and $\boldsymbol{P}_t$ are the radial and tangential components of $\boldsymbol{P}$, respectively; $\boldsymbol{P}_t'$ is the reaction force of $\boldsymbol{P}_t$; $\boldsymbol{P}_r'$ is the reaction force of $\boldsymbol{P}_r$; $\boldsymbol{F}_t$ and $\boldsymbol{F}_n$ are the radial and tangential components of cutting force, respectively.

$$\sum F_X = fp\cos\theta\cos\theta + p\sin\theta + p\cos\left(\frac{\pi}{6}+\theta\right) - fp\cos\theta\cos\left(\frac{\pi}{3}-\theta\right) - p\cos\left(\frac{\pi}{6}-\theta\right) - fp\cos\theta\cos\left(\frac{\pi}{3}+\theta\right) = 0, \tag{4}$$

$$\sum \boldsymbol{M}_o = \boldsymbol{T} - \boldsymbol{T}_f - 3\boldsymbol{P}_t h - 3\boldsymbol{F}_{pt} h = 0, \tag{5}$$

$$\boldsymbol{P} = \frac{\boldsymbol{T} - \boldsymbol{T}_f}{3h(\sin\theta + f\cos\theta)}, \tag{6}$$

$$\boldsymbol{P}_r = \frac{\boldsymbol{T} - \boldsymbol{T}_f}{3h(\tan\theta + f)}. \tag{7}$$

In the upper model, h is the radius of action of the plate wire plane thread, f is the friction coefficient of the contact surface part, F_X is the force in the X direction of the coordinate axis, $\boldsymbol{M}_o$ represents the

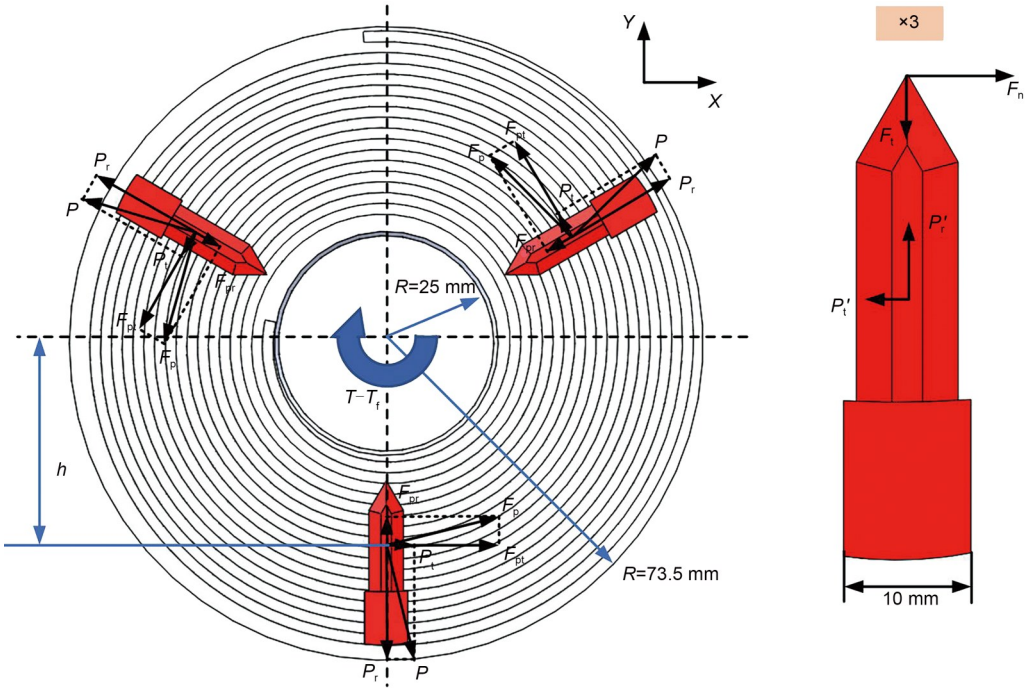

Fig. 12 Force analysis of cutters

torque force on the cutting spiral grooved plate, $\boldsymbol{T}$ is the driving torque, and $\boldsymbol{T}_f$ is the obstruction of the friction moment. By combining the equations, the torque required by the motor can be obtained. The servo motors are selected according to the torque, and other factors (such as control method, power supply voltage, and rated power) that are required.

4.3 Cutting process simulation

Simulation is a standard analysis method. In the process of high-fidelity cutting design, ABAQUS software is used for simulation. On the one hand, the simulation analysis of the cutter cutting process provides the design basis; on the other hand, it also proves the rationality of the design (Yen et al., 2004; Attanasio et al., 2010).

According to the design, a single cut takes 2 min, so the process of a single feed is simulated. The simulation result of a single cutting is shown in Fig. 13. Simplified cutters are used in the simulation, and the number is changed to 4 to achieve symmetrical cutter distribution and to speed-up the calculation. The simulation results show that the cutter can penetrate the hydrate sample wholly and smoothly. It can be concluded from the stress-strain diagram that there is a maximum stress at the tool-tip. With the penetration of the cutting knife, the disturbance to the hydrate in the sample tube increases gradually until the peak of the disturbance (about 105 s) is reached. After cutting, the influence of the tool will fall back to a lower level. The cutter rotates clockwise, and the stress distribution on the tangential plane also rotates in the direction of the cutter movement. Since the sample tube's material is PVC and the strength of hydrate is obviously lower than that of PVC, it is difficult to simulate by setting all the cutting tools to PVC. The disadvantage of this is that it unrealistically increases the difficulty of cutting, but if the whole cutting action is to be completed, the cutting action must be completed under actual conditions (PVC sampling tube containing hydrate).

5 Experiments

5.1 Test process

As shown in Fig. 14, the working process of the core sample pressure maintaining transfer device is as follows:

(A) Connect the gravity sampler and the deep-sea sample high-fidelity processing system via a hoop, turn on the temperature and pressure holding device, and adjust the temperature and pressure of the deep-sea sample processing system to the same point as the sampling point.

(B) Open the ball valve to connect the gravity sampler with the deep-sea sample high-fidelity processing system, start the long-stroke push device, push the grab rod to the sample tube joint, and rotate the grab rod to make the connection between them secure.

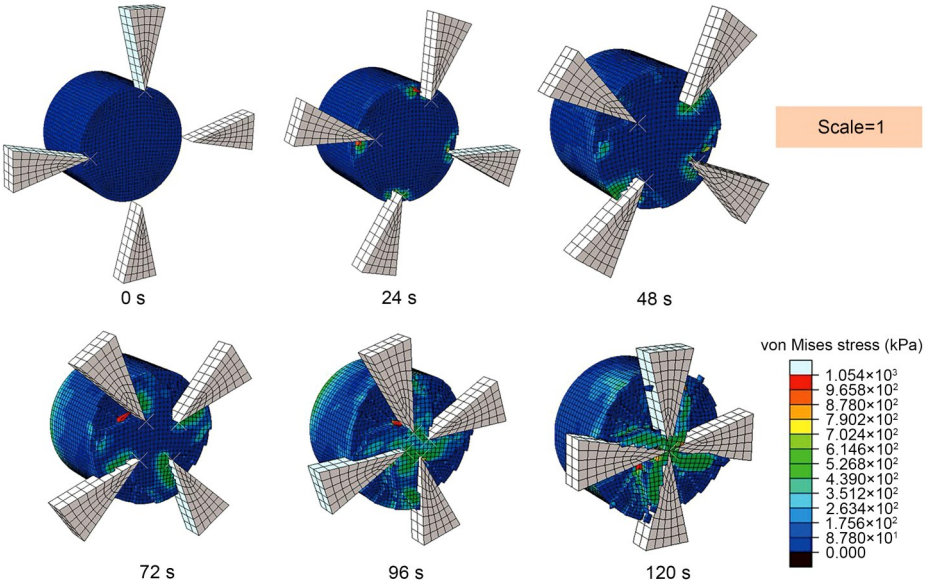

Fig. 13 Single cutting simulation

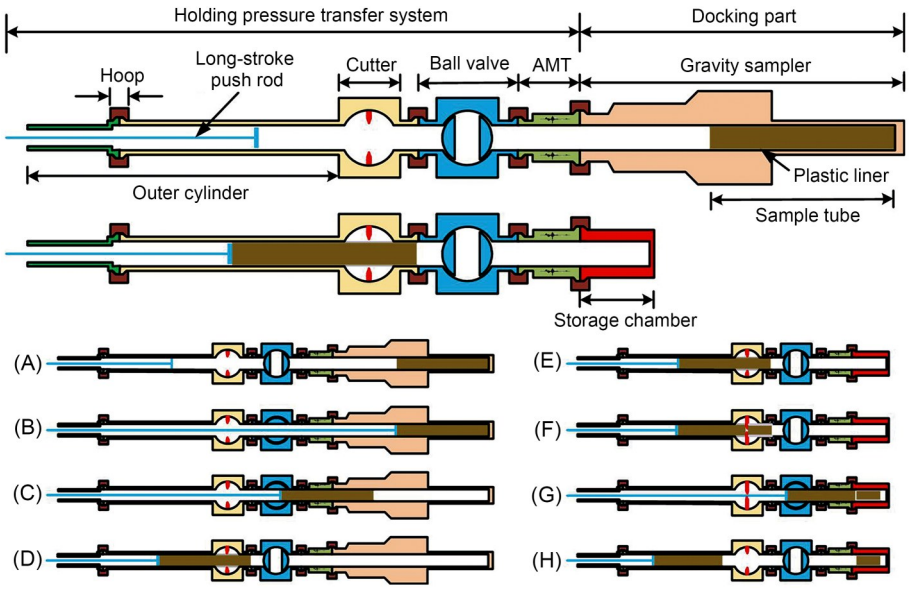

Fig. 14 Hydrate sample processing of the hydrate samples pressure-holding transfer system (AMT: acoustic measurement tank)

(C) Maintain the same temperature and pressure, retract the gripper to the CT, reduce the speed, and rotate the gripper while opening the CT for scanning to obtain the internal structure of the sample.

(D) Wait until the CT scan is complete, continue to retract the gripper with the sample tube to the high-fidelity sample cutting device, and stop retracting. Then close the ball valve.

(E) Open the hoop and disconnect the gravity sampler from the deep-sea sample high-fidelity processing system. Then the sample storage compartment is connected to the deep-sea sample high-fidelity processing system.

(F) Hold the long-stroke pushing device still, open the clamping mechanism of the deep-sea sample high-fidelity cutting device to fix the sample tube, and open the cutting mechanism to cut the sample tube.

(G) Wait for the sample tube to be cut. Open the ball valve and push forward the sample section to be cut as required into the sample storage compartment.

(H) Retract the gripper and close the ball valve. The sample section to be cut is already in the storage compartment. Close the valve in the sample storage compartment and disconnect the clamp. The cutting is completed in one step. Repeat the above steps to cut the sample section again.

To complete the cutting, it is necessary to initialize the cutting device to determine the position of the cutting knife. During the design process, the range of motion of the cutter is determined by the interval of the parameter equation of the Archimedes spiral on the spiral grooved plate, and the upper and lower limits of the interval can be used to limit the cutter. Without a reducer, control the No. 1 motor to rotate to overload, and the knife is centered. To avoid the cutters colliding with each other in error, a 3-mm circumferential safety clearance is set. After the operation of reserved safety clearance is completed, the cutting can be recycled. Table 4 shows the setup parameters for each step. The revolving cutting process includes rotating cutting and returning to the maximum diameter, as shown in Fig. 15.

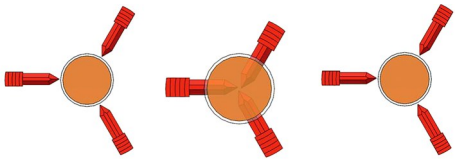

Fig. 15 Complete single cut process schematic

It should be noted that W1 is the speed of cutting of the cutter limit plate, and W2 is the speed of cutting of the spiral groove plate. When the values of W1 and W2 are negative, they all represent the anti-clockwise rotation of the motor. W1+W2 represents the superposition speed, which determines the feed and returns the speed of the cutter. The value of W1+W2 represents rotary feed when it is negative and rotary withdrawal when it is positive.

5.2 On-site cutting effect

We cut at the in-situ pressure and see that the pressure gauge (top left corner in Fig. 16) shows up to 30 MPa, and this pressure is maintained for at least 12 h (Gao et al., 2020). During the test, the team connected ball valves at both ends of the cutting device, pushed the pressure from the top with a pneumatic booster pump, and maintained the pressure with ball valves. The state of the cutting knives inside the high-fidelity cutting device is shown in Fig. 16, uniformly distributed, and due to the compensating design of the length of the cutting knives, the circles formed by the tip of the three cutting knives coincide with the centers of the sample tube. The sample tube cut by the high-fidelity cutting device is shown in the lower right corner of Fig. 16. The cut-out of the sample tube is smooth, and the minimum width of the sample pipe section can be much less than 2 cm, so that almost any length of the sample tube can be cut.

When the inside of the sample tube is filled with sediment, the whole cutting surface and sediment of the sample tube are also very smooth. The cutting surface characteristics can be summarized as follows: smooth cutting surface, smooth incision, little sediment disturbance, and almost no chip residue. Therefore, in general, the cutting effect achieved by the cutting path of the cutter is very satisfactory.

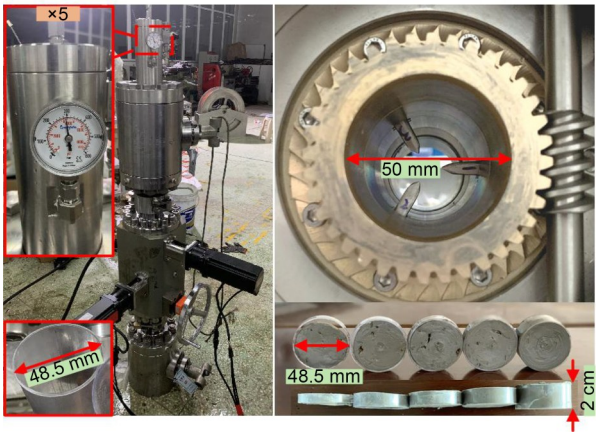

Fig. 16 On-site installation and cutting effect demonstration

6 Discussion

Hydrate samples separated by conventional means generally no longer have the same characteristic properties once they are onshore as they did on the sea floor. Hydrates decompose at elevated temperatures and reduced pressures, so conventional hydrate samples lose their characteristics once they are onshore. Even if some pressure-holding samplers maintain the pressure, the change in temperature and the lack of associated sample transfer and cutting processing devices make it impossible to perform laboratory tests in the same state as on the sea floor.

In this study, a high-fidelity cutting device for in-situ cutting of hydrate sampling tube was designed, mainly based on the principle that the Archimedes spiral is an isometric spiral. The electronic control system controls servo motors to drive the worm gears and worms so that the cutter can move in the spiral groove according to the Archimedes spiral line. This cutter motion path results in less cutting disturbance for the hydrate samples and makes precise control possible due to the determination of the motion path. The sample tube had an outside diameter of 48.5 mm and a total of 10 cuts were made. The cut sections are shown in Fig. 17. Most of the cut sections are very flat, with only two or three of them producing a larger disturbance. In general, the disturbance level of the cut sections is well controlled.

The single cutting time is only 2 min, which achieves high cutting efficiency while maintaining the quality of the cut. In order to save time, the differential speed of tool retraction can be increased to achieve the fastest retraction to the original position within 20 s, so that the single cycle cutting time is 140 s. The whole process is controlled by the upper computer to achieve a rapid cycle of cutting. During the sea trial,

Table 4 Motor setup table for cutting process

Step	Action	Time (s)	W1 (r/min)	W2 (r/min)	W1+W2 (r/min)
1	Cutting knife centering	–	−180	0	−180
2	Reserving a safe distance	9	540	0	540
3	Backing to maximum diameter	30	2700	0	2700
4	Cutting	120	−2295	1620	−675
5	Repeating steps 3 and 4				

Fig. 17 Cutting sections of in-situ sample tubes

the pressure fluctuation of both core holding pressure transfers was 1.04%. In addition to the role of the pressure maintenance system, the good sealing performance of all parts, including the high-fidelity cutting device, jointly achieved this goal, so that the result achieved far exceeded the design goal (a pressure fluctuation of less than 10%).

Thanks to the use of the electronic control system, the control of the servo motors became simple and reliable, and the corresponding cutting function could be better realized. Defining and encapsulating the buttons on the upper computer interface enables one-button cutting and fallback. The upper computer interface can dynamically display the position of the core tube in real time, making it possible to cut any length of sample tube within a section. To avoid cutting into the entire rock, an emergency cutback function was designed to avoid the loss of in-situ environmental pressure due to reloading. The main difficulty in re-calibrating the tool without equipment disassembly is the presence of ambient pressure and unseen material in the equipment. Thanks to the Archimedes spiral, which can be calculated precisely, improvements at the software control level can be made to obtain the desired results.

In April 2021, we conducted a sea trial test in the South China Sea and performed two pressure-holding transfer tests (including many steps such as transfer, cutting, scanning, and sample transfer storage). The first core was processed from 7:04 a.m. to 9:26 a.m. for about 2.5 h, during which the pressure varied from 22.07 to 21.84 MPa, and the pressure fluctuation rate was calculated to be 1.04%. The second core was processed from 10:04 a.m. to 4:36 p.m. for about 6.5 h, during which the pressure varied from 20.18 to 19.97 MPa, and the calculated pressure fluctuation rate was 1.04%. In the PCATS, developed by Geotek Ltd., UK in the HYACINTH program, only 15% pressure range is guaranteed. During China's Twelfth Five-Year Plan period, the pressure fluctuation index of pressure-holding transfer equipment is 20%. Compared with previous products, this equipment has made great progress in respect of pressure fluctuation, and pressure fluctuation is far less than 10% specified in its design. The high-fidelity cutting device designed has reached the current international advanced level in controlling pressure fluctuation. Similar advanced performance is reflected in the control of temperature fluctuations, which do not exceed 0.5 ℃ during sea trials. Because of the function of the automatic temperature control system, the hydrate will not decompose during the cutting process. Under the condition that the temperature and pressure are strongly controlled, the high-fidelity cutting of the hydrate has achieved initial success.

To better build a high-fidelity cutting device system, the corresponding drive motor selection is the key point, so the clamping force is calculated to provide sufficient driving force to make the in-situ cutting go smoothly. Through force analysis, the relationship between the forces required for the cutting tool and the driving torque is obtained. Combined with cutting analysis, the force required for cutting can be calculated and the driving torque can be calculated by establishing the equation. Then the servo motors can be selected according to the transmission characteristics of worm gear and worm. The simulation analysis reduces the difficulty of simulation by assuming all sample tubes as PVC tubes, because the strength of PVC tubes is greater than that of hydrate. The simulation results show that the cutting of a PVC pipe can be realized, and the cutting under real circumstances is possible.

7 Conclusions

This research investigated the mechanical structure design and electrical control system construction of the high-fidelity cutting device. When cutting by mechanical means, the generation of chips is inevitable. The anti-blocking design was included, preventing cutting chips from entering the spirally grooved disk and

causing cutting blockage. Pre-written procedures rather than manual proofreading realized the initialization and step cycle of the cutting process, which improves the convenience dramatically. Besides, accuracy is improved by orders of magnitude compared with a mechanical counter.

The equipment designed in this study can be used for high-fidelity cutting of deep-sea samples, thus providing important technical guarantees for the study of hydrates. It significantly supports research on marine energy and marine sediment cores. The hydrate is disturbed as little as possible, and is maintained as far as possible at its in-situ state.

Acknowledgments

This work is supported by the Key R&D Program of Zhejiang Province (No. 2021C03183), the Key Special Project for Introduced Talents Team of Southern Marine Science and Engineering Guangdong Laboratory (Guangzhou) (No. GML2019ZD0506), and the National Natural Science Foundation of China (No. 2017YFC0307500).

Author contributions

Hai ZHU designed the device mainly. Hai ZHU and Jia-wang CHEN processed the data. Hai ZHU and Zi-qiang REN drafted the manuscript. Pei-hao ZHANG, Qiao-ling GAO, and Chun-ying XU helped organize the manuscript. Xiao-ling LE helped with the simulation analysis of cutting. Kai HE, Peng ZHOU, Feng GAO, and Yu-ping FANG helped design the device. Hai ZHU revised and finalized the paper.

Conflict of interest

Hai ZHU, Jia-wang CHEN, Zi-qiang REN, Pei-hao ZHANG, Qiao-ling GAO, Xiao-ling LE, Chun-ying XU, Kai HE, Peng ZHOU, Feng GAO, and Yu-ping FANG declare that they have no conflict of interest.

References

Attanasio A, Ceretti E, Fiorentino A, et al., 2010. Investigation and FEM-based simulation of tool wear in turning operations with uncoated carbide tools. *Wear*, 269(5-6): 344-350. https://doi.org/10.1016/j.wear.2010.04.013

Dai S, Santamarina JC, 2014. Sampling disturbance in hydrate-bearing sediment pressure cores: NGHP-01 expedition, Krishna–Godavari Basin example. *Marine and Petroleum Geology*, 58:178-186. https://doi.org/10.1016/j.marpetgeo.2014.07.013

Gao QL, Chen JW, Liu JB, et al., 2020. Research on pressure-stabilizing system for transfer device for natural gas hydrate cores. *Energy Science & Engineering*, 8(4):973-985. https://doi.org/10.1002/ese3.562

Hayashi T, Sakurai S, Shibanuma K, et al., 2014. Development of remote pipe cutting tool for divertor cassettes in JT-60SA. *Fusion Engineering and Design*, 89(9-10):2299-2303. https://doi.org/10.1016/J.Fusengdes.2014.04.026

Hoang AQ, Aono D, Watanabe I, et al., 2021. Contamination levels and temporal trends of legacy and current-use brominated flame retardants in a dated sediment core from Beppu bay, southwestern Japan. *Chemosphere*, 266: 129180. https://doi.org/10.1016/j.chemosphere.2020.129180

Hyodo M, Li YH, Yoneda J, et al., 2014. Effects of dissociation on the shear strength and deformation behavior of methane hydrate-bearing sediments. *Marine and Petroleum Geology*, 51:52-62. https://doi.org/10.1016/j.marpetgeo.2013.11.015

Kamruzzaman M, Dhar NR, 2009. Effect of high-pressure coolant on temperature, chip, force, tool wear, tool life and surface roughness in turning AISI 1060 steel. *Gazi University Journal of Science*, 22(4):359-370.

Li JF, Ye JL, Qin XW, et al., 2018. The first offshore natural gas hydrate production test in South China Sea. *China Geology*, 1(1):5-16. https://doi.org/10.31035/cg2018003

Li L, Kishawy HA, 2006. A model for cutting forces generated during machining with self-propelled rotary tools. *International Journal of Machine Tools and Manufacture*, 46(12-13):1388-1394. https://doi.org/10.1016/j.ijmachtools.2005.10.003

Lukin N, Moura RT, Alves M, et al., 2020. Analysis of API S-135 steel drill pipe cutting process by blowout preventer. *Journal of Petroleum Science and Engineering*, 195:107819. https://doi.org/10.1016/j.petrol.2020.107819

Moore MT, Phillips SC, Cook AE, et al., 2020. Improved sampling technique to collect natural gas from hydrate-bearing pressure cores. *Applied Geochemistry*, 122:104773. https://doi.org/10.1016/j.apgeochem.2020.104773

Pang BX, Wang SY, Jiang XX, et al., 2019. Effect of orbital motion of drill pipe on the transport of non-Newtonian fluid-cuttings mixture in horizontal drilling annulus. *Journal of Petroleum Science and Engineering*, 174: 201-215. https://doi.org/10.1016/J.Petrol.2018.11.009

Parkes RJ, Sellek G, Webster G, et al., 2009. Culturable prokaryotic diversity of deep, gas hydrate sediments: first use of a continuous high-pressure, anaerobic, enrichment and isolation system for subseafloor sediments (DeepIso-BUG). *Environmental Microbiology*, 11(12):3140-3153. https://doi.org/10.1111/j.1462-2920.2009.02018.x

Priest JA, Druce M, Roberts J, et al., 2015. PCATS triaxial: a new geotechnical apparatus for characterizing pressure cores from the Nankai Trough, Japan. *Marine and Petroleum Geology*, 66:460-470. https://doi.org/10.1016/j.marpetgeo.2014.12.005

Ren ZQ, Chen JW, Gao QL, et al., 2020. The research on a driving device for natural gas hydrate pressure core. *Energies*, 13(1):221. https://doi.org/10.3390/en13010221

Saelzer J, Berger S, Iovkov I, et al., 2020. In-situ measurement

of rake face temperatures in orthogonal cutting. *CIRP Annals*, 69(1):61-64.
https://doi.org/10.1016/j.cirp.2020.04.021

Toussaint R, 2008. Pipe Cutting Apparatus. US Patent 7406769.

Tsuchiya M, Nomaki H, Kitahashi T, et al., 2019. Sediment sampling with a core sampler equipped with aluminum tubes and an onboard processing protocol to avoid plastic contamination. *MethodsX*, 6:2662-2668.
https://doi.org/10.1016/J.MEX.2019.10.027

Wang Y, Xu TF, Zhang PY, et al., 2020. Experimental investigation of coolant selection and energy efficiency analysis during gas hydrate-bearing sediment freeze-sampling. *International Journal of Refrigeration*, 120: 221-236.
https://doi.org/10.1016/j.ijrefrig.2020.07.027

Ye JL, Qin XW, Qiu HJ, et al., 2018. Preliminary results of environmental monitoring of the natural gas hydrate production test in the South China Sea. *China Geology*, 1(2):202-209.
https://doi.org/10.31035/cg2018029

Ye JL, Qin XW, Xie WW, et al., 2020. The second natural gas hydrate production test in the South China Sea. *China Geology*, 3(2):197-209.
https://doi.org/10.31035/cg2020043

Yen YC, Söhner J, Lilly B, et al., 2004. Estimation of tool wear in orthogonal cutting using the finite element analysis. *Journal of Materials Processing Technology*, 146(1): 82-91.
https://doi.org/10.1016/S0924-0136(03)00847-1

Yi J, Qian YP, Shang ZQ, et al., 2017. Design of cutting head for efficient cutting machine of thin-walled stainless steel pipe. *Procedia Engineering*, 174:1276-1282.
https://doi.org/10.1016/j.proeng.2017.01.302

Yoneda J, Oshima M, Kida M, et al., 2019. Permeability variation and anisotropy of gas hydrate-bearing pressure-core sediments recovered from the Krishna–Godavari basin, offshore India. *Marine and Petroleum Geology*, 108: 524-536.
https://doi.org/10.1016/j.marpetgeo.2018.07.006

Zhang PH, Chen JW, Gao QL, et al., 2019. Research on a temperature control device for seawater hydraulic systems based on a natural gas hydrate core sample pressure-retaining and transfer device. *Energies*, 12(20):3990.
https://doi.org/10.3390/en12203990

Zhao JF, Song YC, Lim XL, et al., 2017. Opportunities and challenges of gas hydrate policies with consideration of environmental impacts. *Renewable and Sustainable Energy Reviews*, 70:875-885.
https://doi.org/10.1016/j.rser.2016.11.269

Zhu H, Chen JW, Lin Y, et al., 2018. A high pressure holding and cutting device for sampling tube of natural gas hydrate. OCEANS 2018 MTS/IEEE Charleston, p.1-4.
https://doi.org/10.1109/OCEANS.2018.8604734

Zhu ZL, Buck D, Guo XL, et al., 2020. Cutting performance in the helical milling of stone-plastic composite with diamond tools. *CIRP Journal of Manufacturing Science and Technology*, 31:119-129.
https://doi.org/10.1016/j.cirpj.2020.10.005